Supplement of The Cryosphere, 14, 3097–3110, 2020
https://doi.org/10.5194/tc-14-3097-2020-supplement

The Cryosphere Open Access EGU

Supplement of

The role of history and strength of the oceanic forcing in sea level projections from Antarctica with the Parallel Ice Sheet Model

Ronja Reese et al.

Correspondence to: Ronja Reese (ronja.reese@pik-potsdam.de)

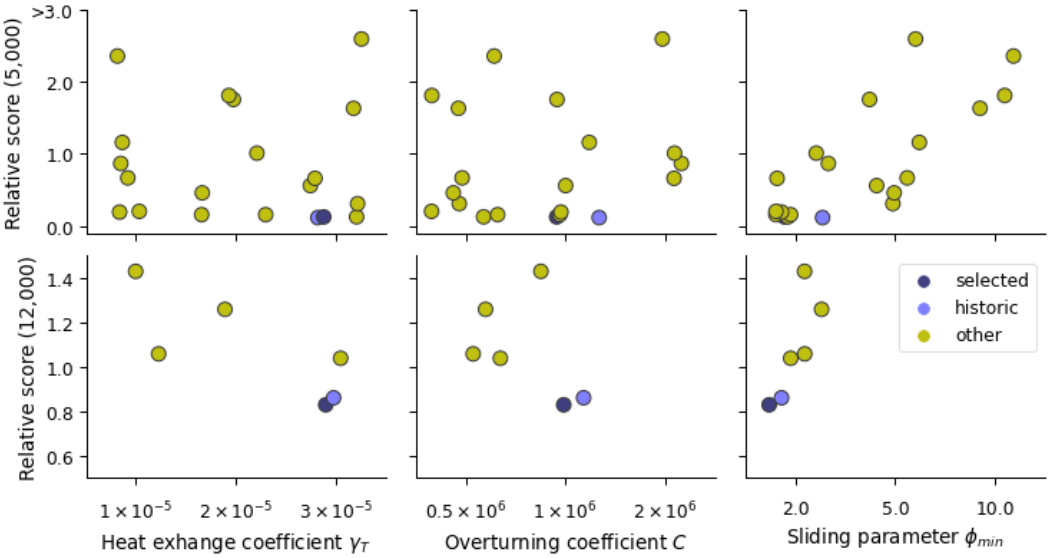

Figure S.1. Comparison of PISM ensemble members with present-day geometry and velocities (Fretwell et al., 2013; Rignot et al., 2011) after (upper row) $5,000$ and (lower row) $12,000$ years of model simulation. Scores are obtained as a product of normalized root mean square deviations from present-day ice thickness and ice speed, deviations in grounded and floating areas and grounding line positions, in line with the approaches presented in (Pollard et al., 2016; Albrecht et al., 2020). A focus is layed on the Amundsen Sea, Filchner-Ronne and Ross ice shelves by testing for those regions in particular. The individual scores are normalized to their median value with smaller scores indicating better fit with observations. The ensemble was done for PICO's heat exchange coefficient (left panels), PICO's overturning coefficient (middle panels) and the minimum till friction angle of the parameterized basal till properties (right panels). After $5,000$ years, the best 5 simulations were continued and re-scored after $12,000$ years to select the best ensemble member, shown in blue here with the state after the historic simulation shown in light blue.

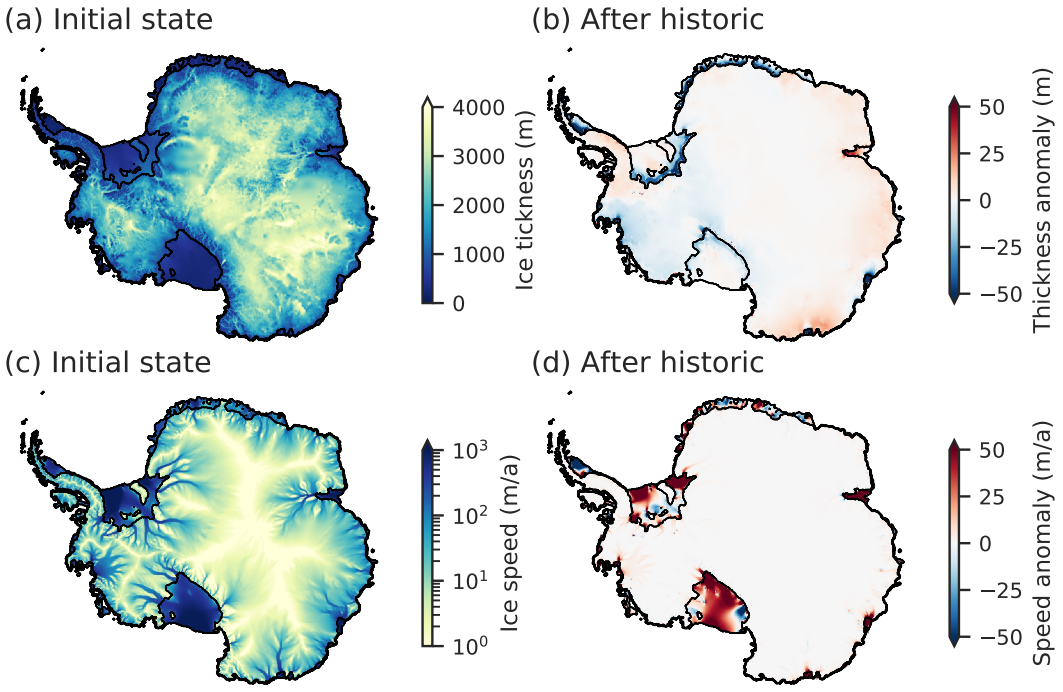

Figure S.2. Modeled ice thickness as in **(a)** present-day pseudo-equilibrium configuration, and **(b)** changes after the historic run. Simulated ice speed in **(c)** pseudo-equilibrium and **(d)** changes after the historic run. Black contours indicate the initial (a,c) and final (b,d) grounding line location.

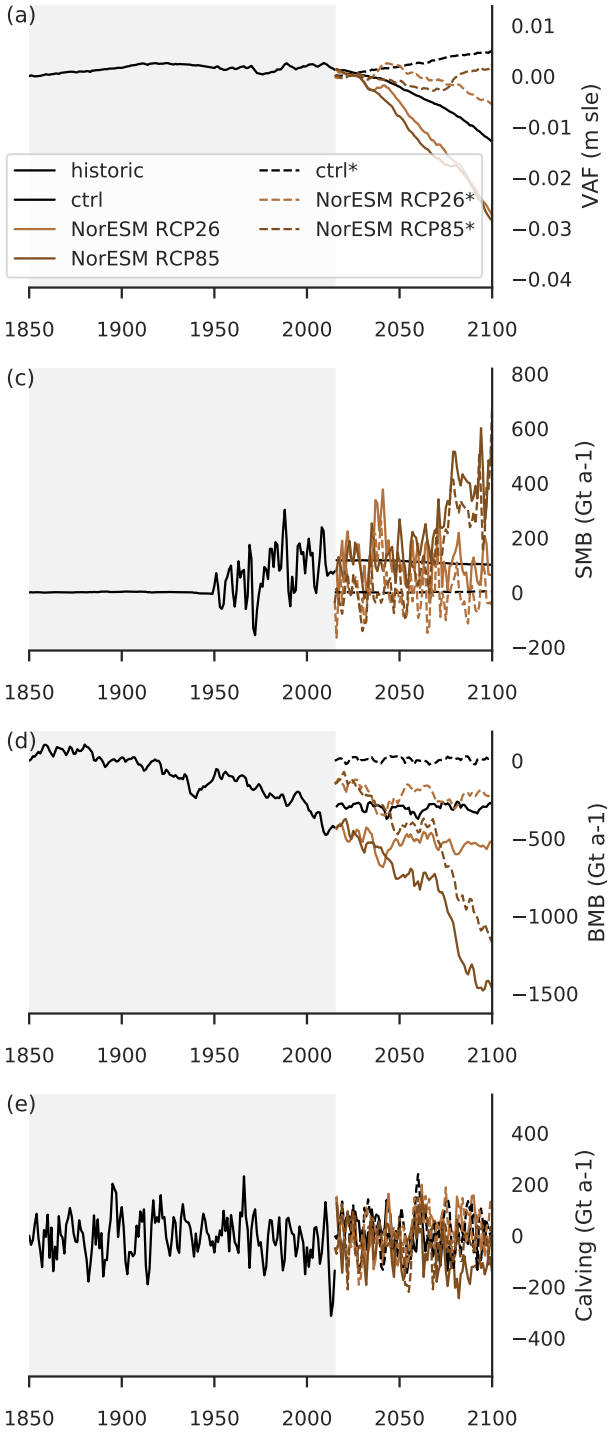

Figure S.3. ISMIP6 experiments with (solid lines) and without (dashed lines) historic initialisation. Shown is the evolution of the (a) volume above flotation, (b) surface mass balance, (c) basal mass balance and (d) calving flux at the ice front relative to the starting condition. Experiments are forced with changes in ocean temperature and salinity and surface mass balance and temperatures from the ISMIP6 protocol experiments no. 1 and 3.

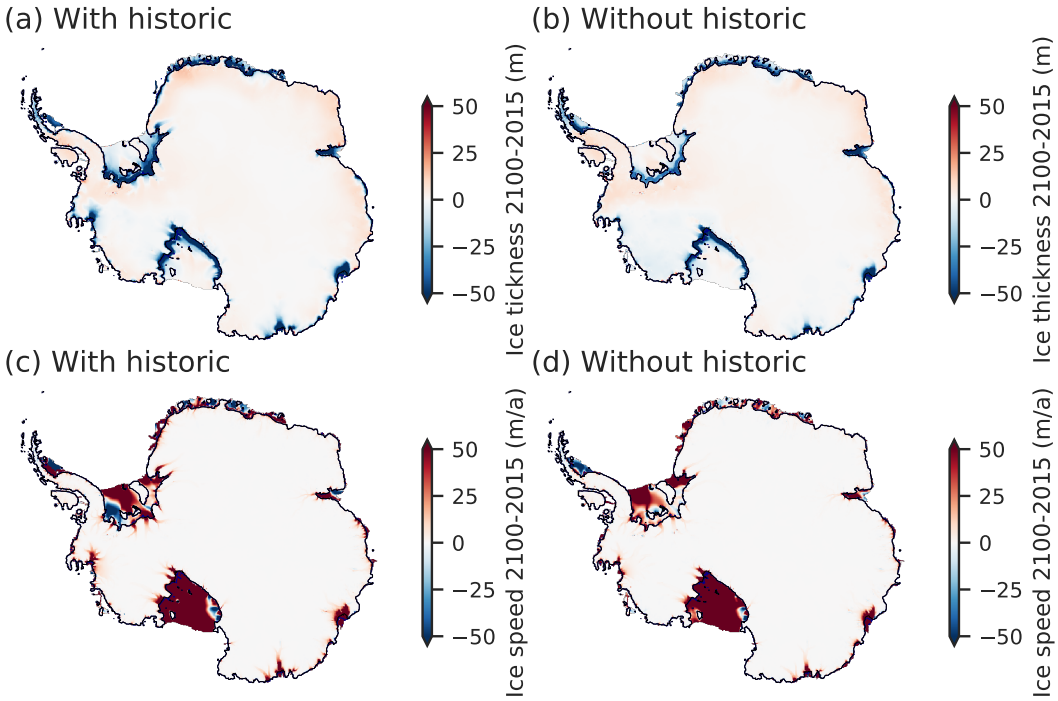

Figure S.4. Changes in ice thickness **(a)** with and **(b)** without the historic run between 2100 and 2015. The corresponding changes in ice speed **(c)** with and **(d)** without the historic run for experiment no. 1 from ISMIP6 (NorESM1-M, RCP8.5).

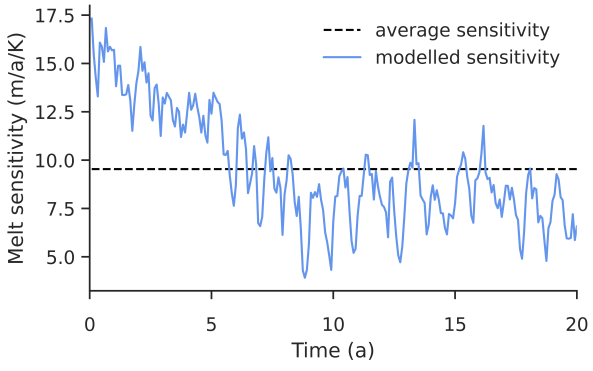

Figure S.5. Sensitivity of sub-shelf melt rates of Thwaites glacier in the coupled simulation from Seroussi et al. (2017). The sensitivity is estimated from the shelf-wide average melt rate in two coupled simulations that differ by initial and boundary ocean temperatures of $0.5\,^{\circ}\mathrm{C}$. The sensitivity might be biased by differently evolving ice-shelf cavities over time.

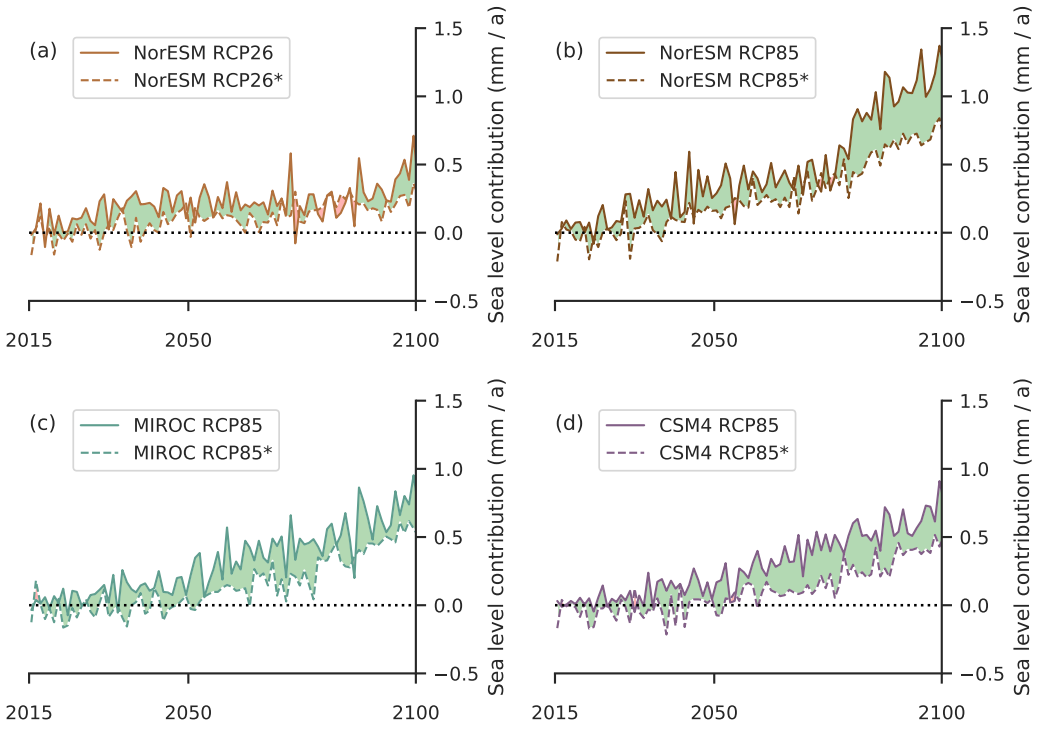

Figure S.6. Rate of sea-level rise between 2015 and 2100. We compare rates of sea-level rise for simulations driven by GCM ocean forcing with the corresponding model specified in the legend. Time periods when sea-level rates are larger in the simulations based on the historic simulation are indicated in green and periods when the simulations starting from the pseudo-steady state induce stronger sea-level rise are indicated in red.

Table S.1. List of all experiments, with INIT being based on the historic simulation starting from INIT*.

MIP	INIT	INIT*
		historic ctrl
		historic
all	ctrl	ctrl*
initMIP	asmb	asmb*
initMIP	abmb	abmb*
ISMIP6	NorESM RCP85	NorESM RCP85*
ISMIP6	MIROC RCP85	MIROC RCP85*
ISMIP6	NorESM RCP26	NorESM RCP26*
ISMIP6	CCSM4 RCP85	CCSM4 RCP85*
LARMIP-2	AP $4\,\mathrm{m\,a^{-1}}$	AP $4\,\mathrm{m\,a^{-1}}$
LARMIP-2	EAIS $4\,\mathrm{m\,a^{-1}}$	EAIS $4\,\mathrm{m\,a^{-1}}$
LARMIP-2	RS $4\,\mathrm{m\,a^{-1}}$	RS $4\,\mathrm{m\,a^{-1}}$
LARMIP-2	AS $4\,\mathrm{m\,a^{-1}}$	AS $4\,\mathrm{m\,a^{-1}}$
LARMIP-2	WS $4\,\mathrm{m\,a^{-1}}$	WS $4\,\mathrm{m\,a^{-1}}$
LARMIP-2	AP $8\,\mathrm{m\,a^{-1}}$	AP $8\,\mathrm{m\,a^{-1}}$
LARMIP-2	EAIS $8\,\mathrm{m\,a^{-1}}$	EAIS $8\,\mathrm{m\,a^{-1}}$
LARMIP-2	RS $8\,\mathrm{m\,a^{-1}}$	RS $8\,\mathrm{m\,a^{-1}}$
LARMIP-2	AS $8\,\mathrm{m\,a^{-1}}$	AS $8\,\mathrm{m\,a^{-1}}$
LARMIP-2	WS $8\,\mathrm{m\,a^{-1}}$	WS $8\,\mathrm{m\,a^{-1}}$
LARMIP-2	AP $16\,\mathrm{m\,a^{-1}}$	AP $16\,\mathrm{m\,a^{-1}}$
LARMIP-2	EAIS $16\,\mathrm{m\,a^{-1}}$	EAIS $16\,\mathrm{m\,a^{-1}}$
LARMIP-2	RS $16\,\mathrm{m\,a^{-1}}$	RS $16\,\mathrm{m\,a^{-1}}$
LARMIP-2	AS $16\,\mathrm{m\,a^{-1}}$	AS $16\,\mathrm{m\,a^{-1}}$
LARMIP-2	WS $16\,\mathrm{m\,a^{-1}}$	WS $16\,\mathrm{m\,a^{-1}}$

AP = Antarctic Peninsula, EAIS = East Antarctica, RS = Ross Sea, AS = Amundsen Sea, WS = Weddell Sea as specified in (Levermann et al., 2020).

Table S.2. Comparison of the PISM-PIK LARMIP-2 contribution and the PISM-PIK ISMIP6 contributions.

	ISMIP6	LARMIP-2
horizontal resolution	8	4
vertical resolution	13-$100\mathrm{m}$	7-$48\mathrm{m}$
initialisation	steady-state, historic	$600\mathrm{a}$ constant climate
sub-grid friction at the GL	yes	yes
sub-grid melt at the GL	yes	no
basal melt rates	PICO	PICO
atmosphere	RACMOv2.3	RACMOv2.3
ocean	WOA18+SCH14	SCH14
Amundsen temperature	-1.25	-0.37
till friction angle	parameterized (ensemble)	optimized
eigencalving	$K = 1 \times 10^{16}\mathrm{ms}$	$K = 1 \times 10^{17}\mathrm{ms}$
thickness calving	threshold $< 50\mathrm{m}$	threshold $< 200\mathrm{m}$
prescribed maximum extent	Bedmap2	none
sliding law	pseudo-plastic exponent $q = 0.75$	plastic ($q = 0$)

References: RACMOv2.3 (Van Wessem et al., 2018), WOA18 (Locarnini et al., 2018), SCH14 (Schmidtko et al., 2014).

References

Albrecht, T., Winkelmann, R., and Levermann, A.: Glacial-cycle simulations of the Antarctic Ice Sheet with the Parallel Ice Sheet Model (PISM)–Part 2: Parameter ensemble analysis., Cryosphere, 14, 2020.

Fretwell, P., Pritchard, H. D., Vaughan, D. G., Bamber, J. L., Barrand, N. E., Bell, R., Bianchi, C., Bingham, R. G., Blankenship, D. D., Casassa, G., Catania, G., Callens, D., Conway, H., Cook, A. J., Corr, H. F. J., Damaske, D., Damm, V., Ferraccioli, F., Forsberg, R., Fujita, S., Gim, Y., Gogineni, P., Griggs, J. A., Hindmarsh, R. C. A., Holmlund, P., Holt, J. W., Jacobel, R. W., Jenkins, A., Jokat, W., Jordan, T., King, E. C., Kohler, J., Krabill, W., Riger-Kusk, M., Langley, K. A., Leitchenkov, G., Leuschen, C., Luyendyk, B. P., Matsuoka, K., Mouginot, J., Nitsche, F. O., Nogi, Y., Nost, O. A., Popov, S. V., Rignot, E., Rippin, D. M., Rivera, A., Roberts, J., Ross, N., Siegert, M. J., Smith, A. M., Steinhage, D., Studinger, M., Sun, B., Tinto, B. K., Welch, B. C., Wilson, D., Young, D. A., Xiangbin, C., and Zirizzotti, A.: Bedmap2: improved ice bed, surface and thickness datasets for Antarctica, The Cryosphere, 7, 375–393, https://doi.org/10.5194/tc-7-375-2013, 2013.

Levermann, A., Winkelmann, R., Albrecht, T., Goelzer, H., Golledge, N. R., Greve, R., Huybrechts, P., Jordan, J., Leguy, G., Martin, D., et al.: Projecting Antarctica's contribution to future sea level rise from basal ice shelf melt using linear response functions of 16 ice sheet models (LARMIP-2), Earth System Dynamics, 11, 35–76, 2020.

Locarnini, R. A., Mishonov, A. V., Baranova, O. K., Boyer, T. P., Zweng, M. M., Garcia, H. E., Reagan, J. R., Seidov, D., Weathers, K., Paver, C. R., and Smolyar, I.: World Ocean Atlas 2018, Volume 1: Temperature, NOAA Atlas NESDIS (Vol. 81), 2018.

Pollard, D., Chang, W., Haran, M., Applegate, P., and DeConto, R.: Large ensemble modeling of the last deglacial retreat of the West Antarctic Ice Sheet: comparison of simple and advanced statistical techniques, 2016.

Rignot, E., Mouginot, J., and Scheuchl, B.: Ice flow of the Antarctic ice sheet, Science, 333, 1427–1430, 2011.

Schmidtko, S., Heywood, K. J., Thompson, A. F., and Aoki, S.: Multidecadal warming of Antarctic waters, Science, 346, 1227–1231, https://doi.org/10.1126/science.1256117, 2014.

Seroussi, H., Nakayama, Y., Larour, E., Menemenlis, D., Morlighem, M., Rignot, E., and Khazendar, A.: Continued retreat of Thwaites Glacier, West Antarctica, controlled by bed topography and ocean circulation, Geophysical Research Letters, https://doi.org/10.1002/2017GL072910, 2017.

Van Wessem, J. M., Jan Van De Berg, W., Noël, B. P., Van Meijgaard, E., Amory, C., Birnbaum, G., Jakobs, C. L., Krüger, K., Lenaerts, J., Lhermitte, S., et al.: Modelling the climate and surface mass balance of polar ice sheets using RACMO2: Part 2: Antarctica (1979-2016), Cryosphere, 12, 1479–1498, 2018.